Article

Bio-inspired "Self-denoising" capability of 2D materials incorporated optoelectronic synaptic array

Check for updates

Molla Manjurul Islam[1,2,5], Md Sazzadur Rahman[3,5], Haley Heldmyer[4], Sang Sub Han[1],
Yeonwoong Jung [1,4] & Tania Roy [1,3] ✉

In in-sensor image preprocessing, the sensed image undergoes low level processing like denoising at the sensor end, similar to the retina of human eye. Optoelectronic synapse devices are potential contenders for this purpose, and subsequent applications in artificial neural networks (ANNs). The optoelectronic synapses can offer image pre-processing functionalities at the pixel itself—termed as in-pixel computing. Denoising is an important problem in image preprocessing and several approaches have been used to denoise the input images. While most of those approaches require external circuitry, others are efficient only when the noisy pixels have significantly lower intensity compared to the actual pattern pixels. In this work, we present the innate ability of an optoelectronic synapse array to perform denoising at the pixel itself once it is trained to memorize an image. The synapses consist of phototransistors with bilayer MoS_2 channel and p-Si/$PtTe_2$ buried gate electrode. Our 7×7 array shows excellent robustness to noise due to the interplay between long-term potentiation and short-term potentiation. This bio-inspired strategy enables denoising of noise with higher intensity than the memorized pattern, without the use of any external circuitry. Specifically, due to the ability of these synapses to respond distinctively to wavelengths from 300 nm in ultraviolet to 2 μm in infrared, the pixel array also denoises mixed-color interferences. The "self-denoising" capability of such an artificial visual array has the capacity to eliminate the need for raw data transmission and thus, reduce subsequent image processing steps for supervised learning.

The demand to process vast amounts of data generated from state-of-the-art, high-resolution cameras has motivated energy-efficient on-device artificial intelligence (AI) solutions. Visual data in such cameras are usually captured in analog voltages by a sensor pixel array, and then converted to the digital domain for subsequent AI processing using analog-to-digital converters (ADCs). Recent research has tried to take advantage of massively parallel low-power analog/digital computing in the form of near- and in-sensor processing, in which the AI computation is performed partly in the periphery of the pixel array and partly in a separate on-board CPU/accelerator, accounting for computing at the edge[1-3]. Unfortunately, high-resolution input images still need to be streamed between the camera and the AI processing unit, frame by frame, causing energy, bandwidth, and

security bottlenecks[4]. For the current state-of-the-art algorithms, the number of input parameters (100's of millions) and memory requirement scale proportionately with the input dimensionality and scales exponentially with the accuracy requirements because of the high quality of the video. Hence, it is impossible to perform AI operations at the edge with the current hardware technology.

Image pre-processing by creating circuits which emulate the retina of the eye has been prevalent for some time[5]. However, their scalability has been low, because of which most of the tasks are performed off-chip. Recent reports demonstrate artificial neural networks (ANNs) using 2D materials (photodiodes using WSe_2)[6] and silicon p-i-n photodiode arrays[7] where in-sensor image processing with multiply and accumulate (MAC) operations

[1]NanoScience Technology Center, University of Central Florida, Orlando, FL, USA. [2]Department of Physics, University of Central Florida, Orlando, FL, USA. [3]Department of Electrical & Computer Engineering, Duke University Pratt School of Engineering, Durham, NC, USA. [4]Department of Materials Science and Engineering, University of Central Florida, Orlando, FL, USA. [5]These authors contributed equally: Molla Manjurul Islam, Md Sazzadur Rahman. ✉e-mail: tania.roy@duke.edu

are realized with photocurrents. The absence of non-volatile memory in most optoelectronic devices for in-pixel (in-sensor) processing precludes the realization of more complex image processing and vision tasks.

Several demonstration of optoelectronic synapses exist in the literature[8]. These reports focus on the modulation of conductance using light pulses. The conductance modulation is the result of persistent photoconductivity (PPC), which is a bane for photodetectors since it prevents the photoconductance to return to the value at dark after light is withdrawn. However, the same phenomenon is useful in optoelectronic synapses, since PPC allows the retention of photoconductance. PPC can be caused by charge trapping due to defects, ion migration, phase changes, and the presence of energy barriers that prevent photogenerated carrier recombination commonly known as photogating effect[9–13]. Most of these reports show the operation of the optoelectronic synapses under UV and visible light[8], with fewer demonstrations of synaptic behavior under IR wavelengths[13,14]. Light pulses with a high intensity compared to state-of-the-art photodetectors are used to potentiate the optoelectronic synapses[15,16]. The optical pulse width applied to potentiate the synapses are reported to be in the range of 10 ms–5 s[15,17–19], which is quite slow considering the current image processing applications. Apart from pair pulse facilitation (PPF), excitatory post synaptic current (EPSC) and short term memory (STM), these works displays the non-volatile memory-capability of the devices. However, the long term memory of these devices are reported to be in the range of several second to a few minutes[20–22]. Besides, most of these report dwell with the performance of individual devices. How these devices can be used for performing image processing tasks is seldom reported[18,23]. We aim to show how optoelectronic synapses as pixels can exhibit built-in image processing functionalities.

Image denoising is one of the essential components in any image processing task. Traditionally, the gaussian smoothing filter for high frequency noise removal, or median filter for salt and pepper noise, along with algorithms like non-local median, wavelet denoising and deep learning-based denoising, are integrated for image denoising operations[24–27]. These are realized with considerable amount of circuitry in the back-pane of displays[28] or energy hungry cloud communications[6]. There are different types of signals present in the natural surroundings. The ability to extract desired information from complicated surroundings is crucial to reduce processing time and energy consumption. The human brain utilizes previous experiences and personal judgment to comprehend the information it perceives from the environment, allowing the visual system to filter out noise signals and selectively process visual data[29]. This means that despite the brain receiving a vast amount of visual information from the environment, the ultimate visual perception typically focuses on a few particular objects in the surroundings, while the other stimuli are eventually disregarded. This is the "self-denoising" capability of the human visual system which is expected to be an inherent property of a bioinspired artificial visual system. Although several bioinspired adaptability characteristics like scotopic and photopic behavior of optoelectronic synapses have been studied[21,22,30], the "self-denoising" capability of an artificial visual system is seldom explored. A few reports exist on the implementation of image denoising using phototransistors. Ma et al. utilized a peripheral control circuit to implement median filtering algorithm to remove salt and pepper noise where the image sensors consist of 619 pixels with 8582 MoS_2 transistors[28]. In a 3×3 array of MoS_2 phototransistors, Dodda et al. used positive gate voltage pulses to erase the memory induced by illumination to remove noise from the images[31]. This scheme, though bio-inspired, would require additional control circuitry for deciphering noise from the original image. Instead of using electrical pulses for depression, Shan et al. uses ultraviolet light pulses for removing noise by the process of depression, which adds complexity to the neuromorphic vision sensor system[32]. With pixels using optoelectronic synapses, noise with intensity much lower than the image can be removed by contrast enhancement, as demonstrated by Zhou et al.[18]. In most reports where noisy images are tested for pattern recognition accuracy, an external computing system is employed for the denoising operation[6]. However, the "self-denoising" capability of an

optoelectronic synapse array used as pixels for image processing has not been explored yet.

In this paper, we develop a bio-inspired scheme to "self-denoise" images at the pixel array without connecting to any external circuitry. Two-dimensional (2D) materials are considered ideal candidates for mid infrared (MIR) optoelectronic devices because of their broadband photosensitive properties and easy integrability[33]. Several materials have been explored including semi-metallic graphene[34] and black phosphorus[35] for MIR photo carrier generation. However the gapless nature of graphene and poor air stability of black phosphorus make them unsuitable in emulating optoelectronic synapse characteristics. Recently discovered metal dichalcogenides, $PtTe_2$[36] and $PtSe_2$[37] has been adopted as viable 2D materials for photocarrier generation in the mid-infrared (MIR) for their ability to transition from a semiconductor to a type-II Dirac semimetal with increasing number of layers, coupled with excellent air stability[13,36,38,39]. Here, we developed individual pixels of the optoelectronic synaptic array by combining an infrared-sensitive $PtTe_2/Si$ as the gate electrode with a UV-visible-sensitive bilayer MoS_2 as the conduction channel, configured as a field-effect transistor (FET). The optoelectronic synapses exhibit short-term and long-term potentiation, similar to biological synapses. By virtue of this property, we demonstrate that if such an array is trained to memorize a pattern and then some noise or any other interferences intend to corrupt its memory, the array has the capacity to nullify the effect of the noise and restore the memorized pattern. Using optoelectronic synapses that respond to light from 300 nm in UV to 2 μm in IR, we demonstrate the "self-denoising" capability using the interplay of short-term and long-term memory. The optoelectronic synapse pixels in a 7×7 array exhibit a significant memory retention of at least 1200 s. The robustness of the array against multi-color interferences is shown in this work, owing to the multi-wavelength detection capability of our devices, which depicts the potential of the device to identify unwanted wavelengths in an incoming pattern and remove its effect. This work illustrates the universal capability of optoelectronic synapses for "self-denoising".

Results

Optoelectronic Synaptic Array with "Self-denoising" Capability

Inspired by the process of learning in humans, we have designed a process for image denoising. When we learn something well, the synapses undergo long-term potentiation (LTP). A strong or frequent stimulus causes this LTP, resulting in long-term memory. A weak or infrequent stimulus either does not potentiate the synapses sufficiently, or causes short-term potentiation (STP), which results in short-term memory. Figure 1a shows a cartoon to illustrate the concept of "self-denoising" process expected from an optoelectronic synapse array. First, the array is trained with a pattern using optical excitation so that the devices respond to the photo-stimuli of the pattern and "learn" it. In other words, the optical stimulus sends the optoelectronic synapses into LTP. This training could also be a part of any other process like pattern recognition or preprocessing of an image, which is beyond the scope of this work. Our scheme requires that the conductance state corresponding to LTP should be substantially higher than the conductance state corresponding to STP. One of the ways to attain this is to train the devices with a longer exposure time compared to the near-zero latency of 200 ms for real-time video streaming[40]. In this work, we implement the long exposure time by means of exposing the arrays to a large number of optical pulses. Another important property for successful "self-denoising" operation is that the LTP period of each synapse should be reasonably long, so that the array can remember the pattern long enough for the conductance states to be read and transmitted to subsequent circuitry for further processing. Now, during this time when the synapses are in LTP, if a noisy image falls on the array, it will potentiate the devices in the array accordingly. In our scheme, we call the process of reading the noisy data on the array as "scanning". It is expected that the "scanning" of the noisy image will occur for a far shorter period than the training process, i.e. the stimulus corresponding to the noise "scanning" will be infrequent or weak compared to the stimulus corresponding to the training process. During the "scanning"
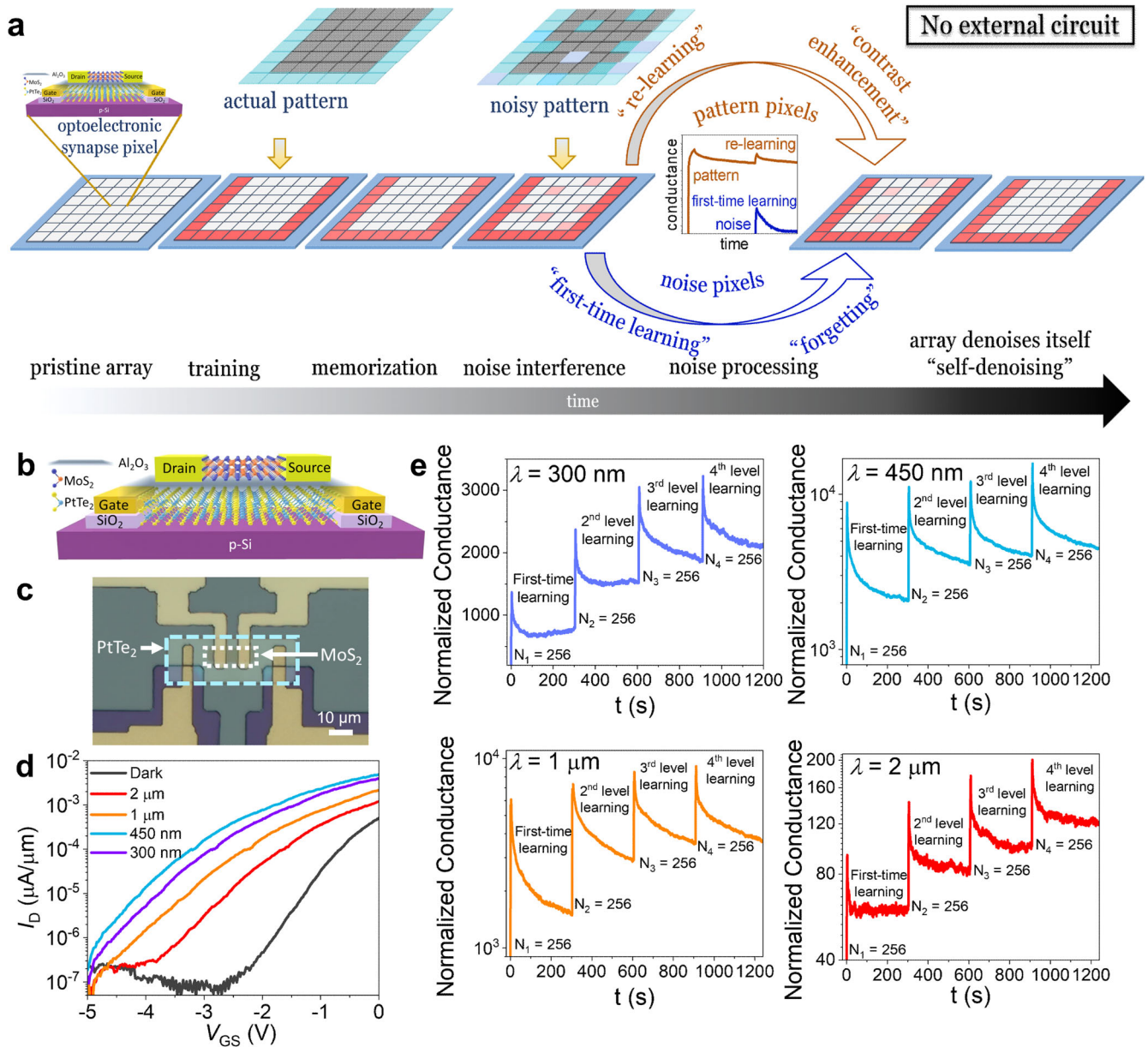
Fig. 1 | Concept of "self-denoising" of an optoelectronic synapse array. a Cartoon of the concept of "self-denoising" process of an optoelectronic synapse array, where the pattern pixels, which are already trained undergo "relearning" process, while the noise pixels experience "first-time learning" resulting in fading of noise by contrast without involving any external circuitry. **b** Schematic and **c** optical microscope image of a 2D materials-based optoelectronic synapse device consisting of MoS_2 as the channel and p-Si/$PtTe_2$ as the buried gate electrode. **d** Transfer characteristics, $I_D - V_{GS}$ of the device in dark and under four wavelengths: 300 nm, 450 nm, 1 μm and 2 μm, showing broadband response and distinct threshold shift for each wavelength. **e** Optical potentiation of the device by applying four bursts of 256 pulses of pulse width 5 ms (effective illumination time = 1.28 s) and optical wavelengths of 300 nm, 450 nm, 1.0 μm and 2.0 μm with memory retention recorded for 300 s after application of each burst of pulses. For all wavelengths, memory gets stronger at each "relearning" level (2nd level learning and onwards). The final memory (conductance) of the devices after four-level learning is more than twice of that of "first-time (first-level) learning", which ensures the capability of the device to sufficiently demonstrate "self-denoising" process.

process, two effects occur: the pattern pixel goes through a second-level learning on top of their previous memory, which we are terming as "relearning", while for the noise pixels, it is a first-time experience, which we will be calling as "first-level learning" or "first-time learning". The "relearning" enhances the LTP state further as every pattern pixel's conductance increases. On the other hand, noise pixels, being first-time potentiated with lesser exposure ("scanning") period, retain lower conductance levels, i.e. only be short term potentiated. The ultimate result is after the noisy image is being "scanned", the pattern pixels get stronger and consequently, the noise pixels fade away in contrast to the pattern pixels' conductance levels. Thus, an optoelectronic synaptic array should be able to

denoise itself for any interference after training. Although the "self-denoising" process might appear as an inherent property for any optoelectronic synapse, the requirement of successful and fast denoising is possible only if the synapse has significant difference between the conductance levels of "first-time learning" and "relearning", established by the difference in conductance levels between its STP state and LTP state respectively. This property governs not only the denoising capability, but also the denoising time.

To establish the "self-denoising" concept, we fabricated a 7 × 7 array of optoelectronic synapse devices. Figure 1b shows the schematic of a multi-wavelength optoelectronic synapse device based on our previous report[13]. The device consists of a bilayer MoS_2 channel acting as an UV-visible

sensitive material during operation[41–44], an Al_2O_3 back gate dielectric, and a p-Si/$PtTe_2$ gate electrode, which is sensitive to infrared (IR) wavelengths[36,38,39]. The details of the chemical vapor deposition (CVD) and device fabrication processes are provided in the Methods section. The materials characterization showing the existence of bilayer MoS_2 are presented in Supplementary Fig. 1a, b. Figure 1c shows the optical image of a device in the array. Figure 1d shows the transfer characteristics of a typical device in the array at $V_{DS} = 1$ V, in dark and under illumination of 300 nm (UV), 450 nm (visible), 1.0 µm (near-IR), and 2.0 µm (IR) wavelengths, with an intensity of 400 µWcm^{-2}. The threshold voltage (V_{th}) shifts negatively under light. The largest negative shift in V_{th} at 450 nm corresponds to the peak of the absorption spectrum of MoS_2[45,46]. The operational principle of the device under light excitation is discussed in our previous work by Islam et al.[11,13].

Now we focus to gain insight about the "learning" and "relearning" of the synapse devices. We potentiated a representative device four times consecutively, each time with a burst of 256 (2^8) optical pulses having a pulse width of 5 ms (effective illumination time = 1.28 s). The memory retention was recorded for 300 s, following which the next burst of pulses was applied. The increasing levels of conductance states with each burst of pulses accounts for the increasing levels of learning by the device, corresponding to "first-time learning" (first level learning), "second level learning (first relearning)" and so on. Figure 1e shows the stepwise optical potentiation and learning of the device at 300 nm, 450 nm, 1.0 µm and 2.0 µm wavelengths with memory retention shown up to 300 s after application of each burst of pulses. V_{DS} is held constant at 1 V and V_{GS} at -2.5 V throughout the experiment. The photoconductance retention occurs only at a negative gate voltage[13]. The memory retention of the device after 300 s of applying one burst of pulses increases as the device is trained multiple times: memory is enhanced from "first-time learning" to second-level learning, from second-level learning to third level learning and so on. It implies that when the devices "relearn" the same information by optical stimulus, there occurs significant difference in the conductance levels between the "first-time learning" and the "relearning" stages. For all wavelengths, the conductance level at the fourth stage (i.e. 3rd "relearning") is over two times higher than the first stage ("first time learning") for our optoelectronic synapse device. The parabolic growth of the memory of the device for the four wavelengths are shown in Supplementary Fig. 2a-d. This is a significant finding for our denoising scheme. We anticipate that this difference between the conductance levels of "first-time learning" and "relearning" should be sufficient to provide the optoelectronic synapse device with the "self-denoising" capability even at a higher wavelength or lower energy photon excitation. In addition, the same principle can be implemented to achieve dynamic motion processing as previously reported[47,48]. As objects approach or leave the synaptic array, the number of illuminated pixels keep increasing or decreasing. Therefore, pixels recieving repetitive train of pulses achieve higher conductance levels compared to the pixels receiving a single train of optical pulses. By sensing these contrasts with additional circuitry, dynamic motion processing can be emulated.

Figure 2a displays an optical image of the 7 × 7 array of the optoelectronic synapse devices described above. The I_D-V_{GS} characteristics of the 49 devices in the array in dark and under illumination with the four light wavelengths of 300 nm, 450 nm, 1 µm and 2 µm are shown in Fig. 2b. All devices show sufficient uniformity to establish the "self-denoising" concept at the array level. The transfer characteristics are distinct for the 4 different wavelengths for all 49 devices, which shows the strength of the array to distinguish between 300 nm, 450 nm, 1 µm and 2 µm light input. This indicates the potential of the devices in color recognition and relevant wavelength-selective artificial visual operations. For all these operations, "self-denoising" capability is an important attribute whenever the input is corrupted by noise or other interferences. Figure 2c represents the tight distribution of V_{th} shifts, ΔV_{th} upon illumination for the 49 optoelectronic synapses in the array. For all wavelengths ΔV_{th} remains within a standard deviation of ~ 0.22 V, implying average device-to-device variability of ~10%.

As mentioned earlier in the manuscript, long-term memory is one of the key performance parameters of optoelectronic synapse array with "self-denoising" capability. It is important that the memory of the devices does not degrade during the pre-processing of an image before moving on to the next process. To evaluate the long-term memory performance of the array, we train the 7 × 7 array to memorize the pattern of "U". Figure 2d shows the capability of the array to memorize the letter "U" for the four different incident light wavelengths of 300 nm, 450 nm, 1.0 µm and 2.0 µm. The training is performed with 1024 light pulses of 5 ms pulse width (effective illumination time = 5.12 s) for each wavelength separately, at V_{GS} = -2.5 V, V_{DS} = 1 V to induce LTP. The long exposure ensures that the pixels exposed to the "U" pattern attain a sufficiently high conductance states to be capable of "self-denoising". After withdrawing the light pulses, the conductance was measured for 1200 seconds by recording I_D in dark. With the application of each light pulse, the devices' photoconductance increases. The photo-conductance state is retained for at least 1200 s after the withdrawal of light. Supplementary Fig. 3 shows the change in photocurrent for individual pixel of the optoelectronic synapse array during the application of pulses and after withdrawal of light for 1200 s. Our results show that the array memorizes the image of the letter "U" at least up to 1200 s after withdrawing the light pulses.

Next, we demonstrate the "self-denoising" operation of the optoelectronic synapse pixel array. The 7 × 7 array was first trained to memorize an image "U" by applying 1024 optical pulses of 5 ms pulse width to induce LTP. The memory status of the array after 100 s is shown in Supplementary Fig. 4. While the array is under LTP, a noisy image of "U" was "scanned" on the trained array with 256 optical pulses of 5 ms pulse width (effective illumination time = 1.28 s) and the change in conductance of the synapse devices in the array was recorded. The scanning time was kept long enough to emulate the worst-case scenario because these images are expected to be "scanned" by any visual system for a short time span. We exposed the optoelectronic synapse array to "U" patterns with Gaussian noise having standard deviations $\sigma = 0.2$ and $\sigma = 0.3$. Thus, the pixels are subjected to varying light intensities, some with intensity higher and some lower than in the original "U" pattern. The first column of Fig. 3 illustrates the noisy input image with 300 nm, 450 nm, 1 µm and 2 µm wavelengths with two different noise levels which is "scanned" on the array for observing "self-denoising" effect. The intensity of the incident light normalized to the standard intensity of 400 µWcm^{-2} (used in the training experiments) is expressed as relative intensity in these figures. After the noisy image "scanning" was completed and the light stimulus is removed, the conductance of each device in the array is measured after 0 s, 10 s, 30 s, and 60 s. First four rows of Fig. 3 (column 2–column 5) represents the contour heatmap plot for "self-denoising" phenomena of the trained array for (a) 300 nm, (b) 450 nm, (c) 1 µm, and (d) 2 µm wavelengths of the optical stimulus in "U" pattern with Gaussian noise level of $\sigma = 0.2$. The contour plot depicts the change in normalized conductance (I_D/I_{OFF}) levels of the devices representing the pixels. The array was able to accurately differentiate between noise and target signals, suggesting its capability to detect complex signals from the environment, and thus suppressing the effect of noise. For a noisy input at 300 nm, 450 nm, and 1.0 µm wavelengths, the array was able to denoise the noisy input image immediately after scanning ($t \sim 0$ s). For 2.0 µm wavelength, the noise pixels were processed with immediate influence-reduction after scanning. However, those pixels were completely denoised within 10 s of the scanning because of the lower conductance level obtained by the devices with this low photon energy. The array shows a clear image of the letter "U", indicating that the noise signals were removed. Note that in the noisy input pattern, there are two noise pixels located at $(5,4)^{th}$ and $(5,6)^{th}$ position in the array, which were subjected to the relative light intensity 0.65 and 0.50 respectively, indicating that those two pixels which received no light input while training were subjected to 65% and 50% of the standard (training) intensity of 400 µWcm^{-2}. The array could denoise itself completely within 10 s for all of the wavelengths, even for those high intensity noise inputs. In addition, the extended time up to 60 s illustrates that there occurs no memory degradation in the "self-denoising" process, rather a contrast enhancement effect occurs due to the "relearning" effect.
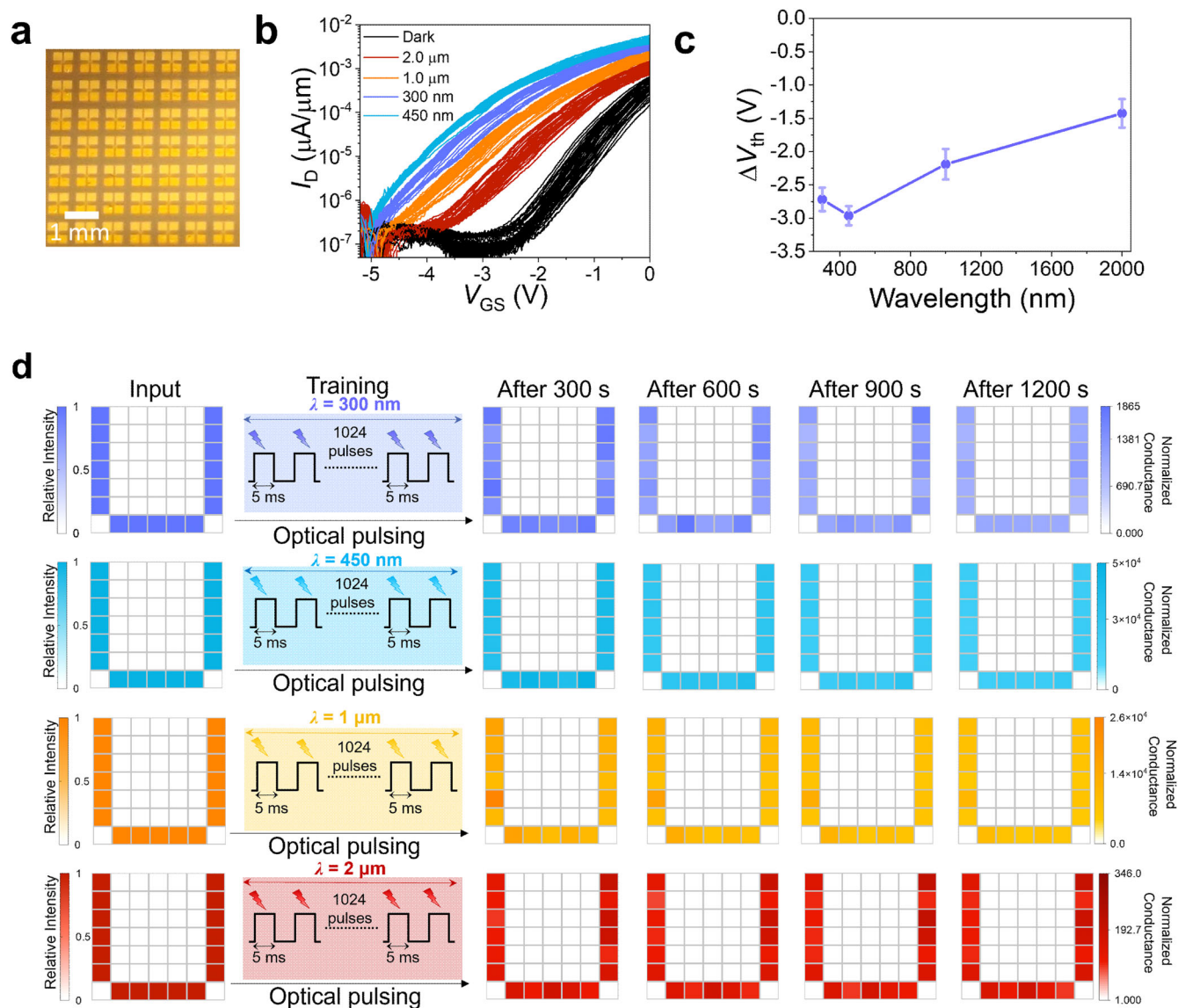
Fig. 2 | 7 × 7 optoelectronic synapse array with excellent memory retention.
a Optical image of optoelectronic synapse array showing 49 devices. **b** Transfer characteristics of all 49 devices in the array in dark and under light (λ = 300 nm, 450 nm, 1 μm and 2 μm) showing distinct threshold voltage shifts for each of the 4 wavelengths. **c** Threshold voltage shift, ΔV_{th} distribution of the 49 devices. **d** Memory retention of the array when it is trained with "U" pattern with 1024 optical pulses of 5 ms pulse width (effective illumination time = 5.12 s) for 300 nm, 450 nm,

1.0 μm, and 2.0 μm wavelength at 300 s, 600 s, 900 s, and 1200 s after withdrawing the pulses. The array shows excellent memory retention capability. In the input side the color represents the relative light intensity of the input sources and at the output side the color indicates the normalized conductance level (I_D / I_{OFF}) of the synaptic devices. I_D, drain current of a device at a particular time; I_{OFF}, average off current of the devices in the array.

Supplementary Figs. 5–8 illustrate the temporal variation of I_D in all pixels at the varying wavelengths.

The same experiment was conducted on the same array for another noisy image of "U" with a higher Gaussian noise level of σ = 0.3. Figure 3e–h represents the 7 × 7 contour heatmap plot of the normalized conductance levels of the array devices for the four wavelengths of 300 nm, 450 nm, 1 μm and 2 μm. The self-denoising effect occurs appreciably within 10 s. Note that one of the noise pixels at $(2,4)^{th}$ position is subjected to a light intensity of 100% of that of the standard (training) intensity of 400 μW cm^{-2}. The array was able to accurately differentiate between noise and target signals and denoised the noisy input image after scanning, eliminating every noise effect within 10 s for all wavelengths. However, for 2 μm wavelengths two noise pixels required 30 s to be removed completely. This is attributed to the low conductance levels attained by the low photon energy of 2 μm wavelength. These results show that even if the LTP conductance state is low, the denoising process occurs successfully but takes longer time compared to

cases where the LTP states are higher. Thus, our MoS$_2$-based optoelectronic synaptic array depicted successful "self-denoising" operation for every noise intensity for a wide range of wavelengths. Supplementary Figs. 9–12 show the temporal variation of I_D for every pixel for the four different wavelengths. The satisfactory performance for 1 μm and 2 μm wavelengths is particularly significant in this work because it indicates the potential of our array for near- and mid-IR sensing operations at room temperature, which are challenging due to low photon energy and responses being masked by thermal noise levels.

In natural environments, various signals can interfere with the target signal and cause distortion. These noise signals can be either single-colored or multicolored and can impact the input. It becomes then imperative that an in-sensor computing system be capable of considering undesired colors as interference/noise and remove its effect. Analyzing the long-term retention levels (conductance) of our array in the previous single-color "self-denoising" section, we devise an algorithm to make our array capable of
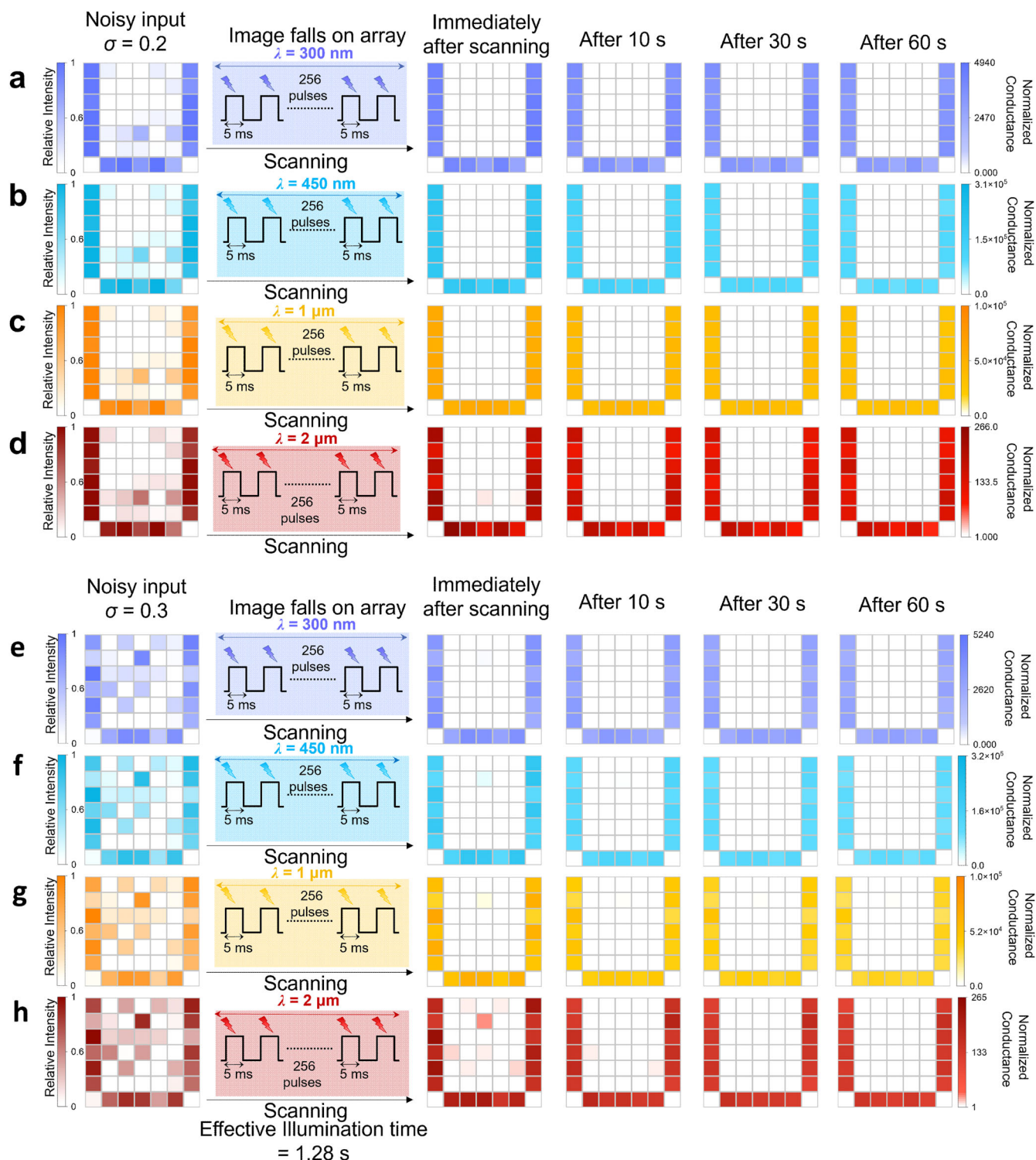
Fig. 3 | "Self-denoising" capability of the synapse pixel array. a Noisy "U" with Gaussian noise of σ = 0.2 (column 1) is "scanned" (allowing the input image to shine the device or reading the image) by the trained 7 × 7 array with 256 optical pulses of 5 ms pulse width (effective illumination time = 1.28 s) at light wavelength of 300 nm. Relative intensity is obtained by normalizing the intensity of light on each pixel to 400 μWcm^{-2}, the intensity used for image memorization. Photoconductance retained after withdrawal of noisy image immediately after scanning (column 2), 10 s after withdrawal (column 3), 30 s after withdrawal (column 4) and 60 s after withdrawal (column 5). Panels **b–d** represent the same information for incident wavelengths of 450 nm, 1 μm and 2 μm, respectively. Panels **e–h** show the input noise pattern and photoconductance retention for "U" input with Gaussian noise of σ = 0.3. For all wavelengths and both noise levels, the array is capable of denoising itself within 10 s (maximum), even for the noise pixels having intensity comparable to pattern intensity, e.g. (2,4)th pixel of noisy image with σ = 0.3 **e–h** has 100% of the pattern intensity, still the array can appreciably eliminate the noise within 10 s for all wavelengths. Conductance values up to 60 s depict no memory degradation during this "self-denoising" process.
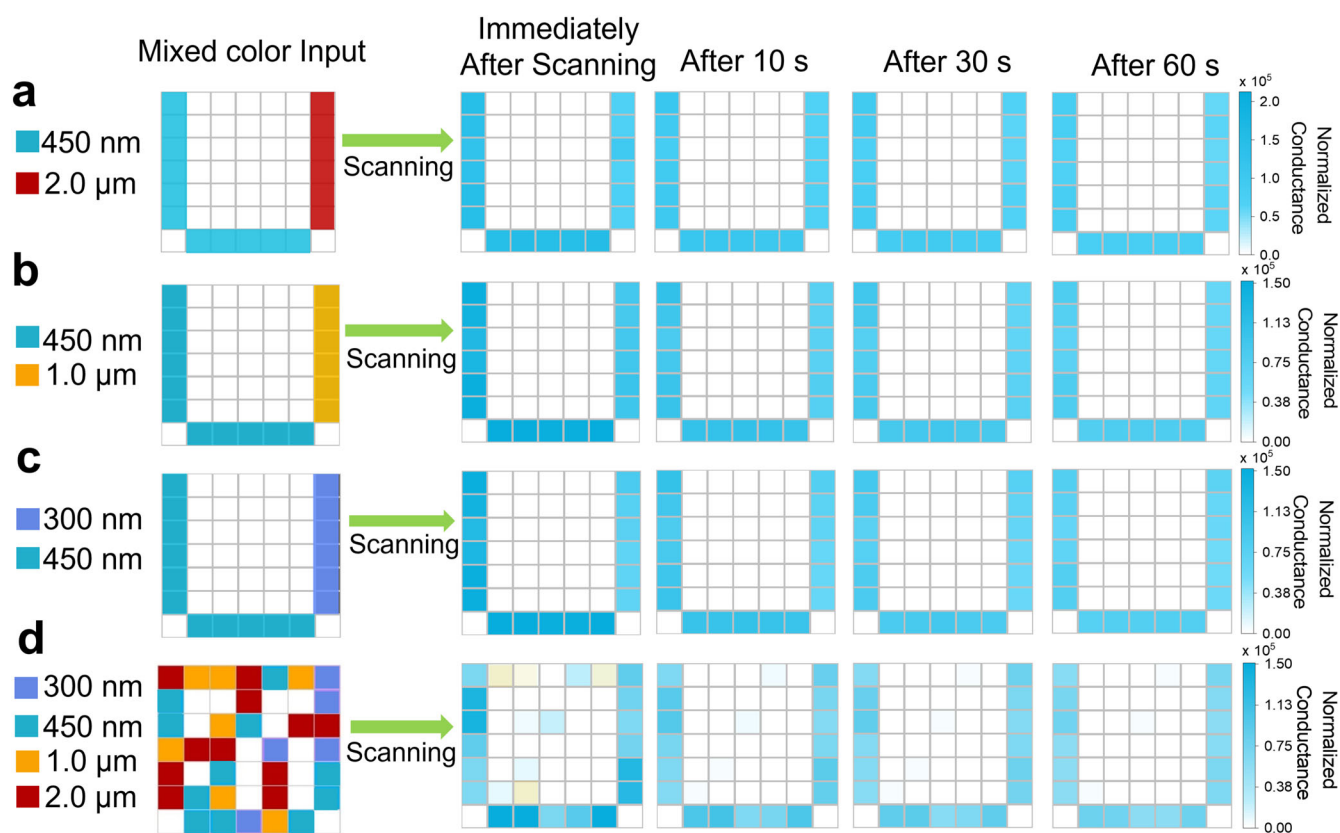
Fig. 4 | "Self-denoising" with mixed-color input. Heatmap plot of the normalized conductance levels of the array, as the trained array is "scanned" (allowing the input image to shine the device or reading the image) with an "U" input corrupted by multi-color interference with 256 pulses having pulse width 5 ms (effective illumination time = 1.28 s), **a–c** only the pattern is corrupted by single-color interference **d** the whole pattern is corrupted by random colored pixels with equal optical intensity (light intensity = 400 μWcm^{-2}). The conductance states of the array is shown immediately (column 2), at 10 s (column 3), 30 s (column 4) and 60 s (column 5) after the scanning pulse removal. For all cases, the array was trained with "U" pattern at 450 nm wavelength light, allowing the conductance levels of the pixel devices to reach high enough to be capable of "self-denoising". For **a–c** the multi-color interference is removed immediately after scanning, while for **d** the array denoised itself completely in ~10 s.

being immune to multicolor interferences, where the array will be able to keep its training information intact if multi-color information intends to corrupt it. The memorization is performed by exposing the array to a pattern at light wavelength of 450 nm, since the LTP states are higher than at other wavelengths with the same intensity and exposure time. This is because bilayer MoS$_2$, which is serving as the UV and visible photosensitive material of the pixel design, has maximum optical absorption near 450 nm wavelength[45]. Now, when a multicolor pattern is "scanned" by the array, the presence of other wavelengths in the pattern do not have an overall impact on the memorized pattern because the LTP levels with other wavelengths are much lower than with 450 nm. The 7 × 7 optoelectronic synapse array was first trained to memorize an image "U" by applying 1024 optical pulses of 450 nm wavelength and 5 ms pulse width. Then a mixed color input image of "U" was scanned over this array with 256 optical pulses of 5 ms pulse width. This experiment was performed for three different mixed color combinations of 450 nm/2.0 μm (column 1 of Fig. 4a), 450 nm/1.0 μm (column 1 of Fig. 4b), and 300 nm/450 nm (column 1 of Fig. 4c) wavelengths. The 7 × 7 contour heatmap plots in the column 2 to column 4 of Fig. 4a–c depicts the changes in normalized conductance of the devices at 0 s (immediately after "scanning"), 10 s, 30 s, and 60 s after withdrawing the scanning pulses. Our array can completely remove this mixed-color interference just after scanning the image (0 s) retaining its original pattern of 450 nm. Next, we tried a more intense multi-color corruption of an image. Column 1 of Fig. 4d shows the noisy image having computer generated randomly positioned color pixels (among 300 nm, 450 nm, 1 μm and 2 μm) corrupting the original "U" pattern, which was used as a multi-color noisy

input. All pixels are exposed to the same light intensities (relative intensity = 1). Figure 4d (column 2–column 5) represents the respective heatmap plot of the pixel conductance variation as a function of time after the light withdrawal. Again, despite having all noise pixels at 100% intensity levels, as well as pattern pixels being corrupted by 100% intense multi-color counterparts, the array was able to accurately differentiate between noise and target signals and denoised the noisy input image after scanning. The noise pixels were processed and reduced immediately after scanning and the noise pixels were completely denoised within 10 s of scanning. Supplementary Figs. 13–16 show the temporal I_D variations of the pixel for all four multi-color interference scenarios. Therefore, the artificial visual array successfully demonstrated the ability to preprocess single colored and multicolored noisy images by removing noise signals to avoid redundant raw data. It was able to produce a clear image of the letter "U", indicating the effectiveness of the "self-denoising" functionality for both single colored and multicolored noisy inputs. Hence, like the human visual system, the array simulated the process of sensing and processing target optical information by itself without any external aid.

Discussion
In summary, we illustrate the innate ability of optoelectronic synapses to perform "self-denoising" at the pixel level. This is possible because of the ability of these devices to undergo short term potentiation when subjected to infrequent inputs and long-term potentiation when subjected to frequent stimuli. When the synapse array is responsive to a broad range of light wavelengths, the pixels can denoise themselves against multi-color

interferences as well. However, the strategy is applicable to supervised learning alone. Further algorithms need to be developed to establish noise-robustness for unsupervised learning. In addition, more investigation needs to be done to enhance the operational speed of the device. First, the CVD growth of MoS_2 can further be optimized to grow larger grain size. Also, the interface between MoS_2 and gate dielectric oxide can be further studied to improve the interface to increase carrier lifetime. However, both approaches might negatively impact the memory retention of the optoelectronic synapse device. To circumvent that, a different device design approach for memory retention can be implemented. Moreover, contact engineering can also improve the operational speed of the device. The devices could be designed with a shorter channel length and larger channel width to improve the ON current, and thereby improve the operational speed of the synapses.

Methods

Materials and device fabrication

The fabrication process flow of the MoS_2 field effect transistor-based multi-wavelength optoelectronic synapse is illustrated in Supplementary Fig. 17. After patterning with photolithography, on a Si substrate, Pt was deposited by e-beam evaporation at a thickness of 6.0 nm followed by lift off. Within a thermal furnace (Blue M Mini-Mite, Lindberg), the Pt deposited Si substrate was placed at the middle of the quartz tube, and the tellurium (Te) powder with a purity of 99.8%, particle size of 200 mesh (CAS No. 13494-80-9), which was obtained from Sigma-Aldrich Inc., was put into an alumina boat. This boat was positioned upstream of the furnace. The substrate with Pt deposited on it, along with the Te powder in an alumina boat, was placed inside a quartz tube. The tube was then pumped to a low pressure of less than 30 millitorr and purged with argon (Ar) gas to eliminate any oxygen and organic materials. Next, the furnace was gradually heated to reach the growth temperature of 400 °C over a period of 50 min. The temperature was held constant at 400 °C for another 50 min before allowing the furnace to cool down naturally to the ambient temperature. Throughout the tell-urization process of Pt, the flow of argon (Ar) gas was kept at approximately 200 standard cubic centimeters per minute (sccm), while maintaining a pressure of approximately 110 mTorr. After patterning with photo-lithography, 200 nm of SiO_2 is deposited by e-beam evaporation followed by liftoff to electrically separate the $PtTe_2$ contact from the bottom Si substrate. Following photolithography patterning, e-beam evaporation was used to deposit 10 nm of Ti and 230 nm of Au as a contact for $PtTe_2$ followed by liftoff. To form the gate dielectric, a layer of 20 nanometers of aluminum oxide (Al_2O_3) was deposited using atomic layer deposition (ALD) technique. The source and drain contacts were created by patterning with pho-tolithography and deposition of Ni/Au using e-beam evaporation with a thickness of 60 nanometers for nickel and 40 nanometers for gold, onto the Al_2O_3 gate dielectric followed by liftoff. Using MoS_2 powder as a precursor, a high-quality and large-area bilayer of MoS_2 was grown using chemical vapor deposition (CVD) in an MTI furnace on a separate Si/SiO_2 substrate with a size of 2.0×2.0 cm^2.

Supplementary Fig. 18a illustrates the process of growing bilayer MoS_2 using chemical vapor deposition (CVD). The MoS_2 powder precursor with a molecular weight of 160.07 was bought from Sigma Aldrich. High quality and large area of bilayer MoS_2 was grown on a Si/SiO_2 substrate with a size of 2.0×2.0 cm^2. The precursor, which was MoS_2 powder, was positioned upstream at the center of the heating zone and the substrate was positioned downstream at 5.0 cm from the precursor. The tube was pumped down to a pressure of less than 15 millitorr and then purged with argon gas to remove any organic materials or oxygen. Ar was used as the carrier gas supplied at a constant rate to maintain pressure of 1.75 Torr. The MoS_2 precursor powder temperature was ramped up to 950 °C at a rate of 10 °C per minute for 95 minutes. The temperature was held constant at 950 °C for another 30 minutes before allowing the furnace to cool down naturally to the ambient temperature. The substrate was kept at 800 °C during the MoS_2 growth process and the whole 2×2 cm^2 substrate was completely covered with bilayer of MoS_2. Supplementary Fig. 18b shows the comparison between the growth parameters for bilayer and monolayer of MoS_2.

Supplementary Fig. 18c represents the optical microscope image of CVD grown (i) bilayer, and (ii) monolayer MoS_2.

Two batches of phototransistor devices were fabricated using CVD grown bilayer and monolayer MoS_2 films to compare optoelectronic synapse device performance. After comparing the electrical characteristics of devices with CVD grown monolayer and bilayer MoS_2 as described in supporting information Supplementary Fig. 19, the bilayer MoS_2 film was transferred onto the source drain contact patterned substrate for 7×7 array of optoelectronic synapse devices. The bilayer MoS_2 was transferred by wet transfer method as explained in Supplementary Fig. 20.

CVD grown bilayer MoS_2 was coated with a thin layer of poly methyl methacrylate (PMMA), followed by drying at room temperature for 12 hours. The PMMA coated sample was then immersed in DI water at an angle of 45^0. Capillary action draws DI water into the substrate/MoS_2 interface, separating the MoS_2 film with the PMMA from the substrate. The MoS_2 film with PMMA was then transferred on the target drain/source contact patterned p-$Si/PtTe_2/Al_2O_3$ substrate and dried for 15 min. The sample was heated on a hot plate at 150 °C for 5 min and the PMMA layer was removed by immersing the sample in acetone for 3 h. The transferred MoS_2 film was then patterned by photolithography and etched in Reactive Ion Etching (RIE) to form the MoS_2 conduction channel.

Device characterization

The Horiba LabRAM HR Evolution Nano Spectrometer was used to perform Raman mapping and photoluminescence spectroscopy with an excitation wavelength of 532 nm. The electrical properties were char-acterized using a Micromanipulator probe station at room temperature in the air, using a Keysight B1500A Semiconductor Device Analyzer. The light source for the experiments was a Newport Quartz Tungsten Halogen lamp, which was split into specific wavelengths using a New-port CS130B-3-MC monochromator. The intensity of light was mea-sured with a THORLABS S401C thermal power sensor, and a Newport 75150 Apex Optical Chopper System was utilized to achieve the desired frequency of light pulses.

Data availability

All data generated and analyzed during this study are either included in the published article itself (or available within the Supplementary Informa-tion files).

References

1. Bong, K., Choi, S., Kim, C., Han, D. & Yoo, H.-J. A low-power convolutional neural network face recognition processor and a cis integrated with always-on face detector. *IEEE J. Solid-State Circuits* **53**, 115–123 (2018).
2. LiKamWa, R., Hou, Y., Gao, Y., Polansky, M. & Zhong, L. in *2016 ACM/IEEE 43rd Annual International Symposium on Computer Architecture (ISCA)*. 255–266.
3. Buckler, M., Jayasuriya, S. & Sampson, A. Reconfiguring the Imaging Pipeline for Computer Vision. *2017 IEEE International Conference on Computer Vision (ICCV)*, 975–984 (2017).
4. Xu, H. et al. in *2020 57th ACM/IEEE Design Automation Conference (DAC)*. 1–6.
5. Kyuma, K. et al. Artificial retinas—fast, versatile image processors. *Nature* **372**, 197–198 (1994).
6. Mennel, L. et al. Ultrafast machine vision with 2D material neural network image sensors. *Nature* **579**, 62–66 (2020).
7. Jang, H. et al. In-sensor optoelectronic computing using electrostatically doped silicon. *Nat. Electron.* **5**, 519–525 (2022).
8. Li, Y. & Shen, G. Advances in optoelectronic artificial synapses. *Cell Rep. Phys. Sci.* **3**, 101037 (2022).

9. Lee, M. et al. Brain-inspired photonic neuromorphic devices using photodynamic amorphous oxide semiconductors and their persistent photoconductivity. *Adv. Mater.* **29**, 1700951 (2017).

10. Pradhan, B. et al. Ultrasensitive and ultrathin phototransistors and photonic synapses using perovskite quantum dots grown from graphene lattice. *Sci. Adv.* **6**, eaay5225 (2020).

11. Islam, M. M., Dev, D., Krishnaprasad, A., Tetard, L. & Roy, T. Optoelectronic synapse using monolayer MoS2 field effect transistors. *Sci. Rep.* **10**, 21870 (2020).

12. Martinez-Martinez, R., Islam, M. M., Krishnaprasad, A. & Roy, T. Graphene–oxide interface for optoelectronic synapse application. *Sci. Rep.* **12**, 5880 (2022).

13. Islam, M. M. et al. Multiwavelength optoelectronic synapse with 2D materials for mixed-color pattern recognition. *ACS Nano* **16**, 10188–10198 (2022).

14. Li, X., Li, S., Tang, B., Liao, J. & Chen, Q. A Vis-SWIR photonic synapse with low power consumption based on WSe2/In2Se3 ferroelectric heterostructure. *Adv. Electron. Mater.* **8**, 2200343 (2022).

15. Li, N. et al. Gate-tunable large-scale flexible monolayer MoS$_2$ devices for photodetectors and optoelectronic synapses. *Nano Res.* **15**, 5418–5424 (2022).

16. Hu, Y. X. et al. Flexible optical synapses based on In2Se3/MoS2 heterojunctions for artificial vision systems in the near-infrared range. *ACS Appl Mater. Interfaces* **14**, 55839–55849 (2022).

17. Gao, S. et al. An oxide schottky junction artificial optoelectronic synapse. *ACS Nano* **13**, 2634–2642 (2019).

18. Zhou, F. et al. Optoelectronic resistive random access memory for neuromorphic vision sensors. *Nat. Nanotechnol.* **14**, 776–782 (2019).

19. Shi, J. et al. A fully solution-printed photosynaptic transistor array with ultralow energy consumption for artificial-vision neural networks. *Adv. Mater.* **34**, e2200380 (2022).

20. Ahmed, T. et al. Fully light-controlled memory and neuromorphic computation in layered black phosphorus. *Adv. Mater.* **33**, e2004207 (2021).

21. Liao, F. Y. et al. Bioinspired in-sensor visual adaptation for accurate perception. *Nat. Electron.* **5**, 84–91 (2022).

22. Meng, J. L. et al. Integrated in-sensor computing optoelectronic device for environment-adaptable artificial retina perception application. *Nano Lett.* **22**, 81–89 (2022).

23. Wan, T. et al. In-sensor computing: materials, devices, and integration technologies. *Adv. Mater.* **35**, 2203830 (2023).

24. Malladi, R. & Sethian, J. A. A unified approach to noise removal, image enhancement, and shape recovery. *IEEE Trans. Image Process* **5**, 1554–1568 (1996).

25. Aslam, N., Ehsan, M. K., Rehman, Z. U., Hanif, M. & Mustafa, G. A modified form of different applied median filter for removal of salt & pepper noise. *Multimed. Tools Appl.* **82**, 7479–7490 (2022).

26. Wink, A. M. & Roerdink, J. B. Denoising functional MR images: a comparison of wavelet denoising and Gaussian smoothing. *IEEE Trans. Med Imaging* **23**, 374–387 (2004).

27. Tian, C. et al. Deep learning on image denoising: an overview. *Neural Netw.* **131**, 251–275 (2020).

28. Ma, S. et al. A 619-pixel machine vision enhancement chip based on two-dimensional semiconductors. *Sci. Adv.* **8**, eabn9328 (2022).

29. Berns, G. *Iconoclast: A neuroscientist reveals how to think differently*. (Harvard Business Press, 2010).

30. Jin, C. et al. Artificial vision adaption mimicked by an optoelectrical In(2)O(3) transistor array. *Nano Lett.* **22**, 3372–3379 (2022).

31. Dodda, A. et al. Active pixel sensor matrix based on monolayer MoS2 phototransistor array. *Nat. Mater.* **21**, 1379–1387 (2022).

32. Shan, X. Y. et al. Plasmonic optoelectronic memristor enabling fully light-modulated synaptic plasticity for neuromorphic vision. *Adv. Sci.* **9**, e2104632 (2022).

33. Long, M. et al. Room temperature high-detectivity mid-infrared photodetectors based on black arsenic phosphorus. *Sci. Adv.* **3**, e1700589 (2017).

34. Wang, X., Cheng, Z., Xu, K., Tsang, H. K. & Xu, J.-B. High-responsivity graphene/silicon-heterostructure waveguide photodetectors. *Nat. Photonics* **7**, 888–891 (2013).

35. Chen, X. et al. Widely tunable black phosphorus mid-infrared photodetector. *Nat. Commun.* **8**, 1–7 (2017).

36. Shawkat, M. S. et al. Scalable van der Waals two-dimensional PtTe2 layers integrated onto silicon for efficient near-to-mid infrared photodetection. *ACS Appl Mater. Interfaces* **13**, 15542–15550 (2021).

37. Zhao, Y. et al. High-electron-mobility and air-stable 2D layered PtSe2 FETs. *Adv. Mater.* **29**, 1604230 (2017).

38. Lai, J. et al. Photocurrent response of type-II Dirac semimetal PtTe2. *2d Mater.* **7**, 034003 (2020).

39. Zeng, L. et al. Van der Waals epitaxial growth of mosaic-like 2D platinum ditelluride layers for room-temperature mid-infrared photodetection up to 10.6 μm. *Adv. Mater.* **32**, 2004412 (2020).

40. *Guide to ultra-low latency & real-time video streaming for IP Cameras. Rhombus (2021). Available at*: https://www.rhombus.com/blog/guide-to-ultra-low-latency-ip-cameras-for-live-video-streaming/. (Accessed: 17th February 2024).

41. Han, P. et al. Ambient effects on photogating in MoS2 photodetectors. *Nanotechnology* **30**, 284004 (2019).

42. Wang, S. et al. A photoelectric-stimulated MoS2 transistor for neuromorphic engineering. *Research* **2019**, 1618798 (2019).

43. He, H. K. et al. Photonic potentiation and electric habituation in ultrathin memristive synapses based on monolayer MoS2. *Small* **14**, 1800079 (2018).

44. Kim, S.-G. et al. Infrared detectable MoS2 phototransistor and its application to artificial multilevel optic-neural synapse. *ACS nano* **13**, 10294–10300 (2019).

45. Castellanos-Gomez, A., Quereda, J., van der Meulen, H. P., Agraït, N. & Rubio-Bollinger, G. Spatially resolved optical absorption spectroscopy of single-and few-layer MoS2 by hyperspectral imaging. *Nanotechnology* **27**, 115705 (2016).

46. Yalon, E. et al. Temperature-dependent thermal boundary conductance of monolayer MoS2 by Raman thermometry. *ACS Appl Mater. Interfaces* **9**, 43013–43020 (2017).

47. Zhou, Y. et al. Computational event-driven vision sensors for in-sensor spiking neural networks. *Nat. Electron.* **6**, 870–878 (2023).

48. Chen, J. et al. Optoelectronic graded neurons for bioinspired in-sensor motion perception. *Nat. Nanotechnol.* **18**, 882–888 (2023).

Acknowledgements

Author contributions

M.S.R. conceived the "self-denoising" idea. T.R. directed the research. H.H. performed the MoS$_2$ synthesis and S.H. conducted the PtTe$_2$ synthesis under the guidance of Y.J. M.M.I. fabricated the devices. M.M.I. and M.S.R. performed the electrical characterization. M.M.I. performed the Raman mapping and photoluminescence spectroscopy of bilayer MoS$_2$ conduction channel. M.S.R., M.M.I., and T.R. performed the data analysis. M.M.I., M.S.R., and T.R. wrote the manuscript with input from all authors. M.M.I and M.S.R. contributed equally to this work.

Competing interests

The authors declare no competing interests.

Additional information

Supplementary information The online version contains supplementary material available at https://doi.org/10.1038/s41699-024-00458-9.

Correspondence and requests for materials should be addressed to Tania Roy.

Reprints and permissions information is available at http://www.nature.com/reprints

Publisher's note Springer Nature remains neutral with regard to jurisdictional claims in published maps and institutional affiliations.